SCIENTIFIC REPORTS

OPEN

SUBJECT AREAS:
NANOPHOTONICS AND PLASMONICS
NANOSCALE MATERIALS

Received
30 June 2014

Accepted
2 September 2014

Published
26 September 2014

Correspondence and requests for materials should be addressed to S.K.R. (physkr@phy.iitkgp.ernet.in)

# Multifunctional Au-ZnO Plasmonic Nanostructures for Enhanced UV Photodetector and Room Temperature NO Sensing Devices

Narendar Gogurla, Arun Kumar Sinha, Sumita Santra, Santanu Manna & Samit Kumar Ray

Department of Physics, Indian Institute of Technology Kharagpur, 721302, India.

**In this study we report the enhancement of UV photodetection and wavelength tunable light induced NO gas sensing at room temperature using Au-ZnO nanocomposites synthesized by a simple photochemical process. Plasmonic Au-ZnO nanostructures with a size less than the incident wavelength have been found to exhibit a localized surface plasmon resonance (LSPR) that leads to a strong absorption, scattering and local field enhancement. The photoresponse of Au-ZnO nanocomposite can be effectively enhanced by 80 times at 335 nm over control ZnO. We also demonstrated Au-ZnO nanocomposite's application to wavelength tunable gas sensor operating at room temperature. The sensing response of Au-ZnO nancomposite is enhanced both in UV and visible region, as compared to control ZnO. The sensitivity is observed to be higher in the visible region due to the LSPR effect of Au NPs. The selectivity is found to be higher for NO gas over CO and some other volatile organic compounds (VOCs), with a minimum detection limit of 0.1 ppb for Au-ZnO sensor at 335 nm.**

Metal nanostructures have attracted substantial interests for applications ranging from medical diagnostics to optoelectronic devices because of their localized surface plasmon resonance (LSPR) in the presence of external light[1–7]. The LSPR arises from light induced collective oscillation of free electrons, leading to strong absorption, scattering and local field enhancement in metallic nanostructures. These resonance characteristics are highly sensitive to the composition, size and morphology of nanostructures. Recently, the novel properties of these nanostructures have been explored for UV photodetectors with an enhanced performance[8], attributed to the plasmonic scattering effect of Ag nanoparticles. Several wide band gap semiconductors including GaN[8], $TiO_2$[9], ZnO[10], etc., have been studied for UV detectors. The attractive electrical and optical properties of zinc oxide (ZnO) has made it to be a promising candidate for applications in photovoltaic, photoconductor, light emitting diodes (LEDs) and gas sensors[11–15]. ZnO has emerged as a potential alternative for GaN for UV detection because of the availability of native substrates with higher exciton binding energy (60 meV).

Recently, the detection of nitrogen oxides such as $NO_2$ and NO has become a research focus due to the environmental problems like greenhouse gas effect and some side effects on human body such as breathing, itching, asthma etc. Traditionally, oxide sensors, which are operated at higher temperatures, have been used to detect these gases[16–18]. A lot of advancement on ZnO based gas sensors has been made in terms of higher responsivity, lower cost and capability of detecting several gases[19–22]. In spite of the advantages, the operation of ZnO gas sensors is limited to higher temperatures (100–400°C). Several methods have been employed to reduce the operating temperature of ZnO sensors e.g. noble metal doping[23], ultra violet (UV) illumination[24], micro-electro-mechanical system fabrication etc[25]. Photo-induced gas sensing measurements offer new opportunities to improve the performance of gas sensor operating at room temperature. There are several reports[24,26] on UV induced room temperature gas sensing properties of ZnO and other metal oxides. Mun et al.[27] reported the enhanced $NO_2$ sensing properties of Au functionalized ZnO nanosheet using UV light. Zhai et al.[28] reported the gas sensing properties of CdS/ZnO nanocomposite using visible light at room temperature.

In this paper, we report the enhancement of UV detection and wavelength-tunable photo-induced gas sensing at room temperature using plasmonic Au-ZnO nanocomposites. The multifunctional Au-ZnO nanocomposite is prepared by a simple photoreduction method to fabricate the device on platinum (Pt) coated interdigitated electrode substrates. The performance of the plasmonic Au-ZnO device has been studied in comparison to

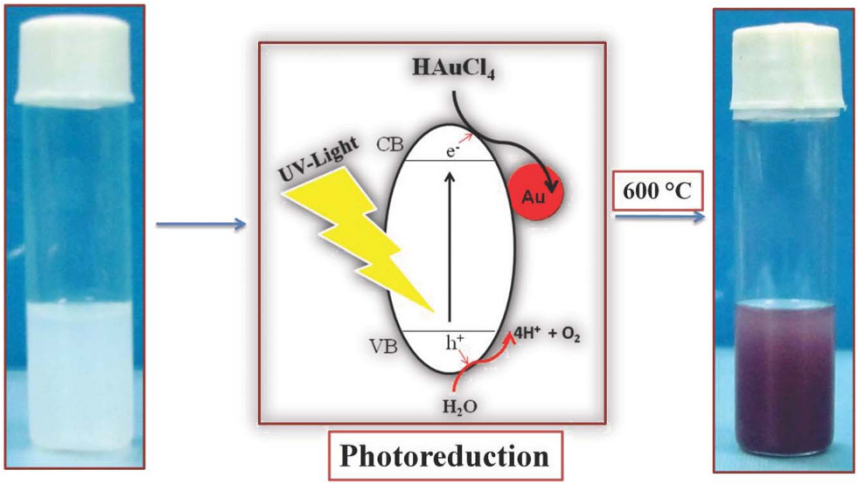


**Figure 1** | **Schematic diagram showing the synthesis of Au-ZnO nanocomposite by photoreduction.**

control ZnO. The mechanisms for enhanced UV responsivity and selective NO detection activated by the photoconductive Au-ZnO nanocomposite are discussed, which may lead to new opportunities in the plasmonic enhanced multifunctional device applications.

## Results and Discussion

The Au-ZnO nanocomposite has been prepared by a simple photoreduction method followed by annealing. The photo-generated electrons from ZnO under UV illumination reacted with $HAuCl_4$ to form Au nanoparticles (NPs) on the surface of ZnO, as shown schematically in Figure 1. Figure S1 shows the field emission scanning electron microscopy (FESEM) images of ZnO and Au-ZnO nanocomposites. The micrograph S1a shows the formation of ZnO nanosheets. The FESEM image in Figure S1b, reveals the formation of spherical shaped Au NPs on the surface of ZnO nanosheets. Figure 2 shows the transmission electron micrograph and diffraction pattern of the synthesized Au-ZnO nanocomposites. As shown in Figure 2a, the spherical Au NP is well attached to the ZnO nanosheet. The observed size distribution of the Au NPs is in the range of 10–50 nm (Supplementary Figure S2). Figure 2b and 2c represents the selected area electron diffraction pattern (SAED) of Au NPs and ZnO nanosheet, respectively. The SAED pattern of Au NPs exhibits circular rings corresponding to (111), (200) and (220) crystallographic planes revealing their polycrystalline nature. The SAED image of ZnO nanosheet shows hexagonal spot patterns, which can be indexed to $(\bar{1}100)$, $(01\bar{1}0)$, $(10\bar{1}0)$, $(\bar{1}010)$ and $(11\bar{2}0)$ planes.

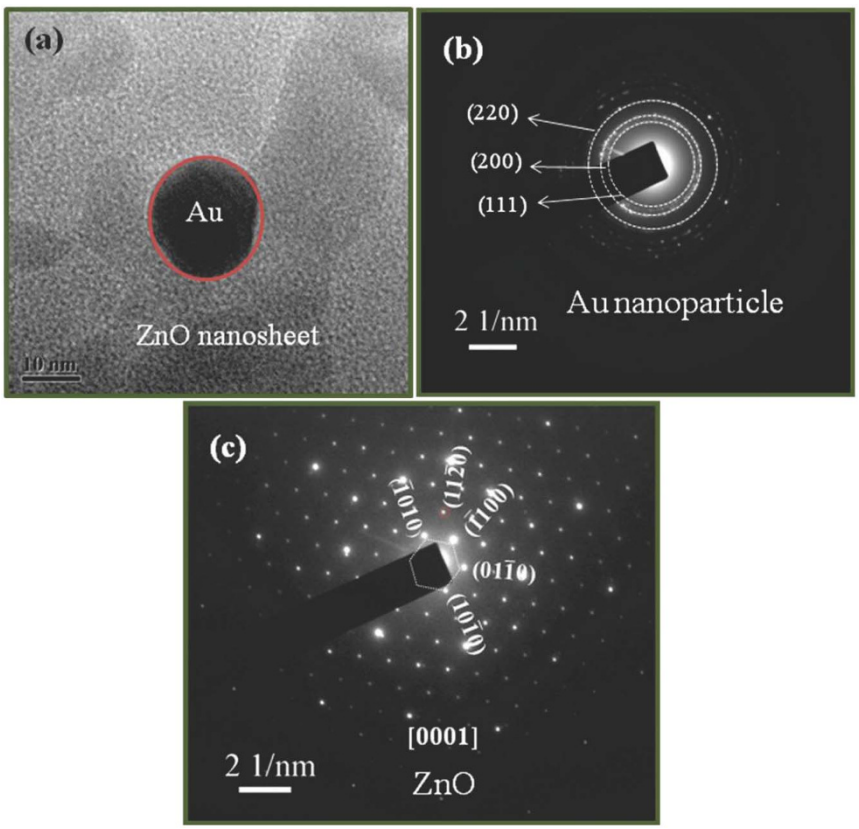


**Figure 2** | **(a) Typical TEM micrograph of Au-ZnO nanocomposite (b) SAED pattern of Au nanoparticle (c) SAED pattern of ZnO nanosheet.**

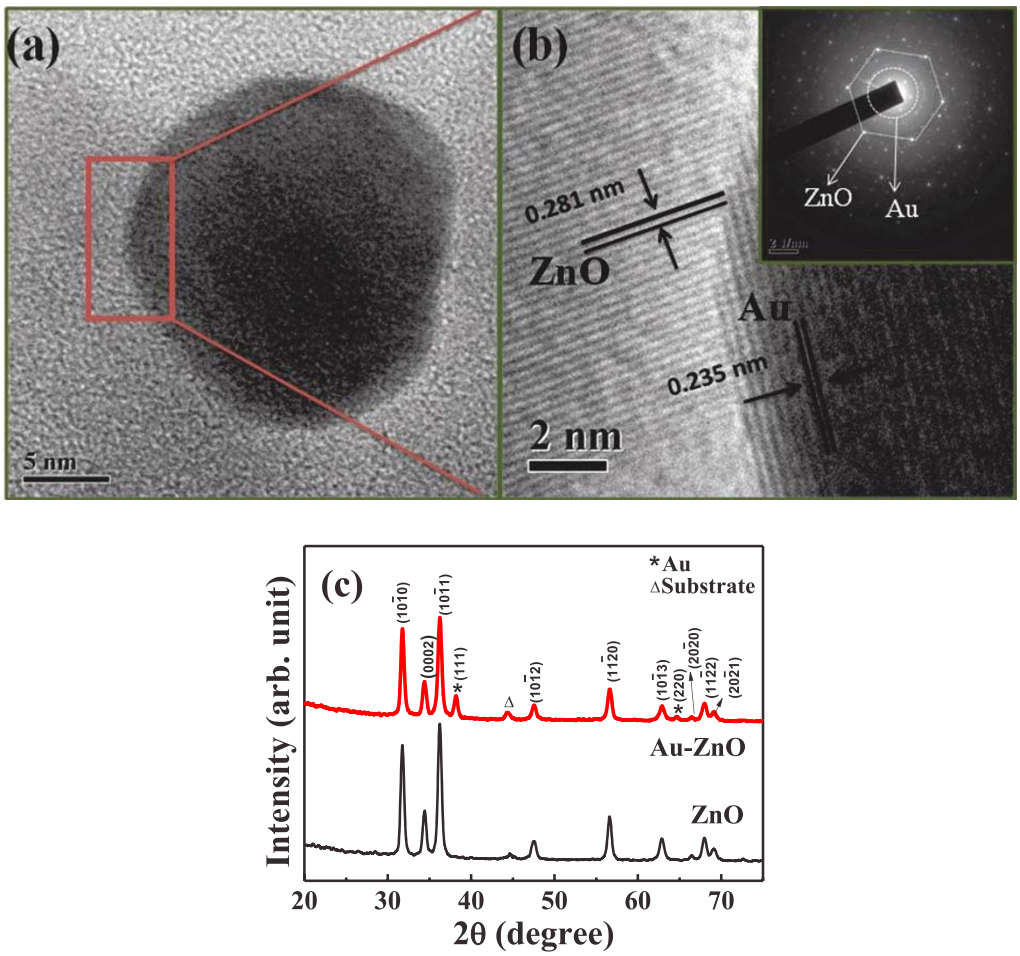


**Figure 3** | (a) HRTEM image of Au-ZnO nanocomposite. (b) HRTEM image showing the lattice fringes of Au and ZnO. The inset shows the combined SAED pattern of Au-ZnO nanocomposite. (c) XRD spectra of ZnO and Au-ZnO nanocomposite annealed at 600°C.

Figure 3a shows the high resolution TEM image of Au-ZnO nanocomposite. Figure 3b presents the lattice fringes of Au-ZnO nanocomposite, from which the interplanar spacing is found to be 0.281 nm and 0.235 nm, for ZnO ($\bar{1}$100) and Au (111) planes, respectively. The corresponding SAED pattern is shown in the inset of Figure 3b, exhibiting the diffraction patterns for both ZnO and Au. The study indicates the formation of Au-ZnO nanocomposites without any intermixing. The structural evolution of ZnO and Au-ZnO nanocomposite has also been examined from the XRD spectra, as shown in Figure 3c. The spectra clearly reveal the formation of well crystalline hexagonal wurtzite phase ZnO. However, the Au-ZnO nanocomposite depicts two additional peaks associated with the face centered cubic phase of metallic Au. The XRD result is in consistent with the HRTEM measurements.

The core level XPS spectra of ZnO nanostructures and Au-ZnO nanocomposites are shown in Figure 4. As shown in Figure 4a, the observed Zn $2p_{1/2}$ and $2p_{3/2}$ binding energy peaks at 1045 and 1020 eV, respectively, remain same for pure ZnO and Au-ZnO nanocomposite. This further corroborates that the Zn exists in the $Zn^{+2}$ state in both the ZnO and Au-ZnO nanocomposite, without any compound formation in the latter. The O 1s spectrum shown in Figure 4b also indicates no change in the chemical state of O in Au-ZnO nanocomposite as compared to ZnO. The binding energy of O 1s is resolved into two peaks i.e., 530 and 531.2 eV. The peak at 530 eV represents the O 1s level in the ZnO, which is surrounded by Zn atoms. On the other hand, the peak at 531.2 eV is attributed to the formation of zinc hydroxide with chemisorbed oxygen species[29]. The core level binding energy of Zn-3p and Au 4f electrons are shown in Figure 4c. The Zn-3p binding energy for both the Au-ZnO and ZnO samples is resolved into several peaks correspond to Zn $3p_{3/2}$ (88.1 eV), Zn $3p_{1/2}$ (91.1 eV) Au $4f_{7/2}$ (82.90 eV) and $4f_{5/2}$ (86.65 eV), as shown in Figure 4c. As seen in Figure, the binding energy peak position of Zn-3p is same in all samples, indicating unchanged chemical state of Zn with the inclusion of Au on the surface of ZnO. The binding energy of Au 4f is found to be shifted towards lower values compared to pure gold ($4f_{7/2} \sim 84.00$ eV and $4f_{5/2} \sim 87.71$ eV)[30], as shown in Figure 4c. This shift is due to the formation of negatively charged Au nanoparticles without any chemical bonding with ZnO. The donor level of ZnO is nearly equal to the Fermi level of Au (5.4 eV). Therefore, there may be possibility of electron transfer from ZnO to the Au, leading to the increment in the charge density on the surface of Au NPs[31].

Figure S3 shows the optical absorption spectra of Au NPs of different sizes prepared by Frens method[32]. A red shift in the plasmon band with increasing particle size is observed. The plasmon band location depends on the particle size, charge density of Au NPs, inter particle spacing and surrounding dielectric medium. Figure 5 shows the absorption spectra of ZnO and Au-ZnO nanocomposites with different reaction time. The spectrum of Au-ZnO sample clearly illustrates two peaks: one at the UV region around 380 nm and the other in the visible region around 550 nm. The peak in the UV region originates from the band edge absorption of ZnO and that in the visible range is due to the surface plasmon absorption of Au NPs. The characteristic plasmon peak of Au-ZnO nanocomposite is observed to be broad in the visible region. The broad visible absorption of Au-ZnO nanocomposites does not show any shift in the plasmon band

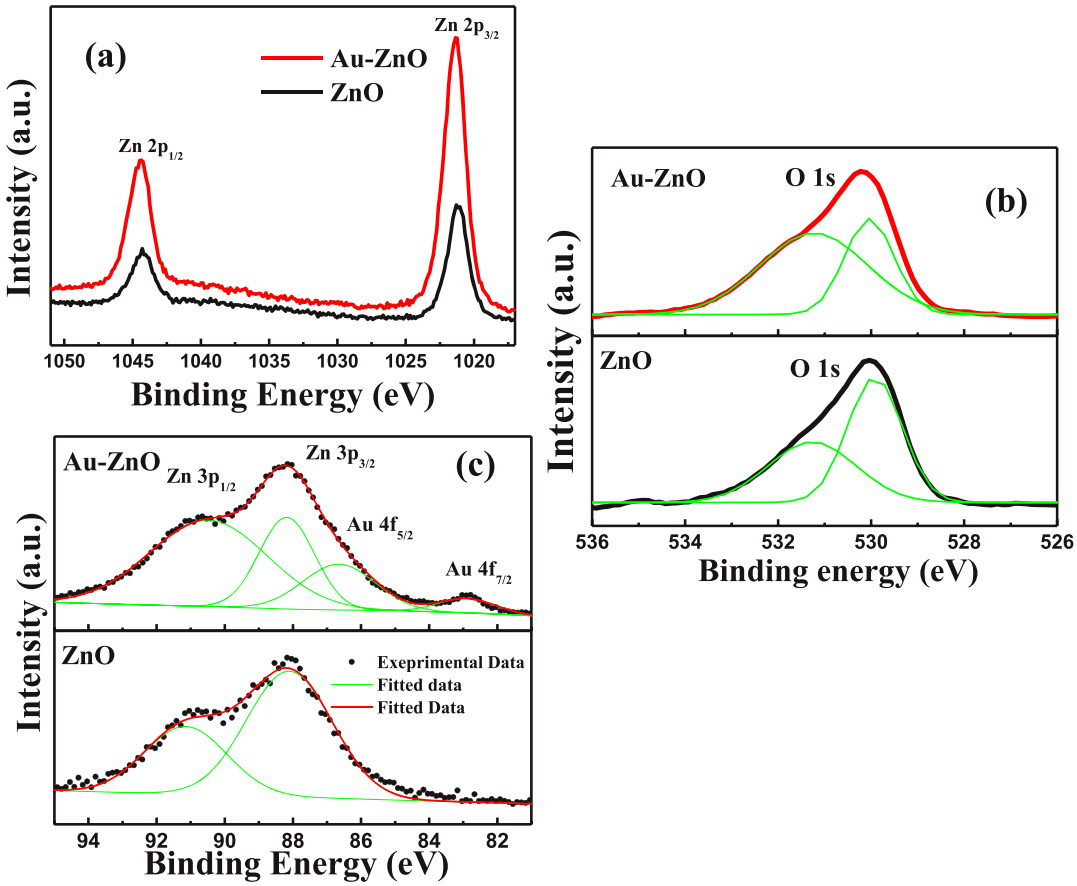


**Figure 4** | XPS core level spectra of ZnO and Au-ZnO nanocomposites showing binding energy of (a) Zn 2p, (b) O1s and (c) Zn 3p and Au 4f electrons.

with increasing reaction time due to the wide particle size distribution, as shown in Figure S2. The Au-ZnO nanocomposites prepared with a typical reaction time of 10 hrs has been used for the device applications reported here.

**UV Photodetection.** The photoresponse of Au-ZnO nanocomposite along with the control ZnO sample has been studied under illumination using a lateral photoconductor device configuration shown in Figure 6a. Typical I-V characteristics of ZnO and Au-ZnO devices measured under dark and UV illumination are shown in Figure 6b. In both the devices, the dark current is found to be low (4.84 nA for ZnO and 5.2 nA for Au-ZnO at 5 V) and an abrupt increase in the current is observed under illumination with UV light. The photoconductivity of Au-ZnO device is found to be enhanced over the ZnO device under the same measurement condition. Figure 6c shows the photoresponse spectra of both the devices at 5 V bias. The responsivity ($R_\lambda$) of the devices has been calculated using[33],

$$R_\lambda = \frac{\Delta I}{PA} \tag{1}$$

where $\Delta I$ is the difference between the photo-excited and dark current, $P$ is the power density irradiated on the sample and $A$ is the area of the device. The responsivity has been estimated using a calibrated detector. The Au-ZnO nanocomposite device shows enhanced photoresponse as compared to ZnO over a broad wavelength range. The responsivity of Au-ZnO is significantly higher for the wavelength range 300–350 nm and gradually decreases when the device is illuminated with a longer wavelength. The peak responsivity of Au-ZnO device is enhanced by 80 times at 325 nm wavelength over ZnO, as seen in Figure 6c. This enhancement in photo-responsivity is higher as compared to the reported value for the Ag-GaN based photoconductors[8].

The origin of enhanced UV photoresponse of Au-ZnO nanocomposite device over the ZnO one may result from the inter-band transition of Au d-band electrons in the UV region or photogenerated hole trapping in the Au nanoparticles. The filled d-band in Au below the Fermi level provides large number of electrons for inter-band transition under UV light illumination[34,35]. Upon UV excitation, the d-band electrons of Au NPs are excited to the conduction

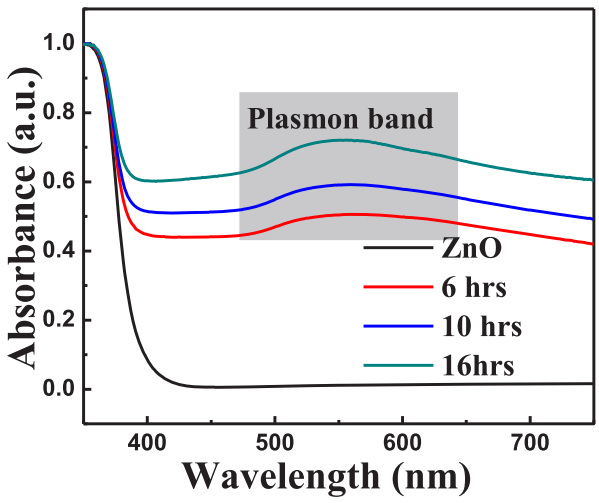


**Figure 5** | UV-Vis absorption spectra of ZnO and Au-ZnO nanocomposite with different reaction time.

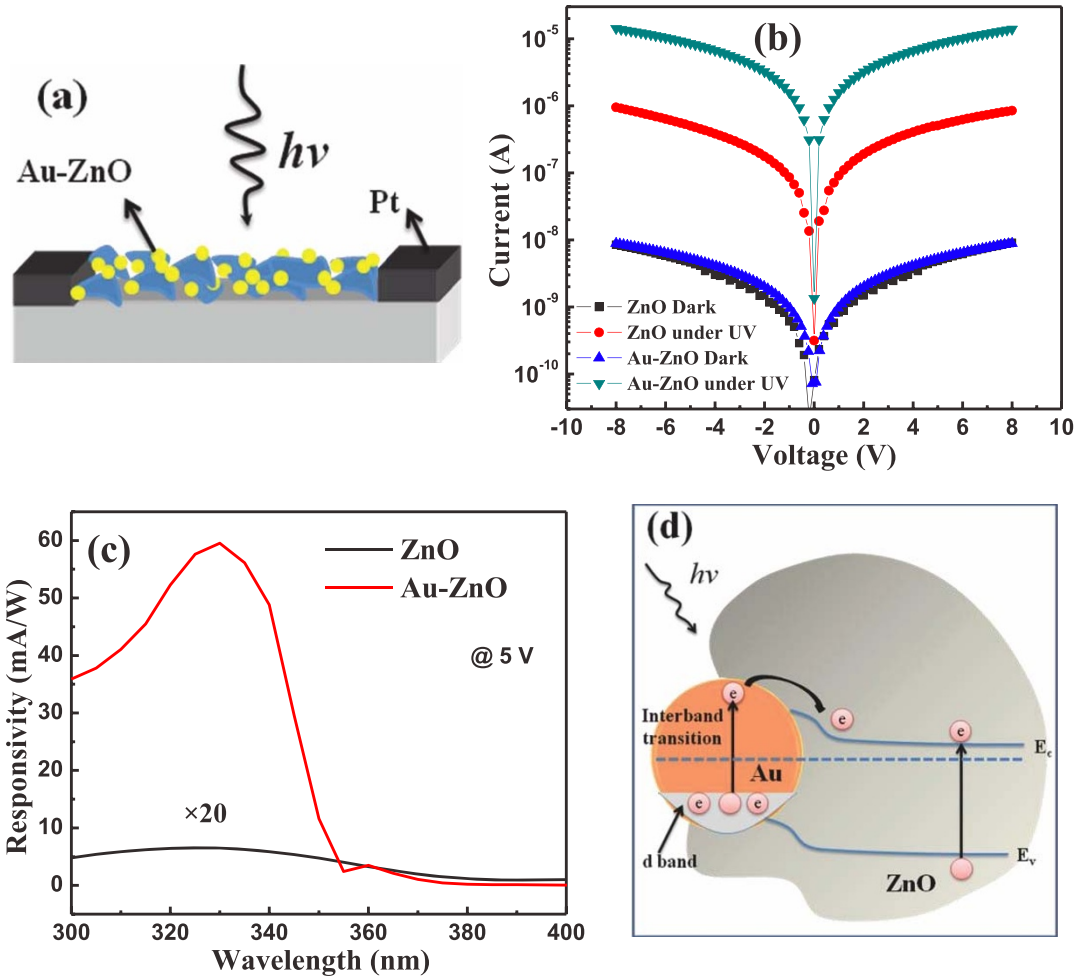


**Figure 6** | (a) Schematic illustration showing the device diagram of Au-ZnO. (b) I-V characteristics of ZnO and Au-ZnO devices under dark and UV illumination. (c) Photoresponse of ZnO and Au-ZnO devices in the UV region at 5 V. (d) Schematic illustration of charge transfer process in Au-ZnO.

band and transfer to ZnO side due to the presence of electric field at the metal-semiconductor junction formed between Au and ZnO, resulting in higher photoconductivity. In case on ZnO, the responsivity in UV region is attributed to the band edge absorption and is much lower than the Au-ZnO nanocomposite. The absorption and transfer processes are schematically shown in Figure 6d. On the other hand, it may also possible that the photogenerated holes in the ZnO can be trapped by the Au nanoparticles, which notably suppress the electron-hole recombination in the device[36]. Due to this, more number of charge carriers collected by the electrodes thus enhances the photoresponse in the UV region.

Figure 7a shows the typical I-V characteristics of ZnO and Au-ZnO devices under dark and visible illumination. As observed in Figure, the Au-ZnO device shows an increase in the photocurrent, while the current in ZnO remains same upon visible illumination. This is expected since the band gap of ZnO is much higher than the incident energy. Figure 7b shows the photoresponsivity in the visible wavelength range for both the samples. As seen in Figure, the Au-ZnO shows a broad photoresponse in the visible region in well agreement with the absorption spectrum of Au-ZnO sample. The responsivity in case of control ZnO is negligible. The visible photoresponse has been reported in many Au functionalized wide band gap materials and was reported to be originated from the localized surface plasmon resonance (LSPR) effect of Au NPs[37,38]. Figure 7c shows the schematic illustration of the mechanism for visible photoresponse of Au-ZnO by charge transfer from Au to the ZnO. As seen in Figure, under visible illumination, the electrons are excited to the surface plasmon band of Au as the decay channel of LSPR is followed by the electron transfer to the ZnO. The visible photo-activation of wide band gap materials due to plasmonic effect can be useful for many applications[39–41].

**Gas sensing devices.** Figure S4 shows the schematic of the gas sensing setup used in the present study, the details of which have been discussed in the methods and measurements. Wavelength tunable gas sensing measurements have been carried out in Au-ZnO nanocomposite in presence of NO, CO and other volatile organic compounds (VOCs) using photo-resistance measurements. The sensor response (S) for a particular gas NO, is calculated using the relation,

$$S(\%) = \frac{(R_{NO} - R_{air})}{R_{air}} \times 100 \qquad (2)$$

where $R_{NO}$ is the resistance of Au-ZnO film in presence of NO gas and $R_{air}$ is the film resistance in presence of dry air. Figure 8a shows the dynamic gas sensor response of Au-ZnO nanocomposite device upon exposure to NO with different concentrations in dry air, for two different incident wavelengths (335 and 350 nm) at room temperature. The response of the control ZnO sample is also presented for comparison at a particular wavelength (335 nm), as shown in Figure 8a. The timing in the pulse sequence is maintained as 'ON' for 15 min and 'OFF' for 15 min. Upon exposure to NO gas,

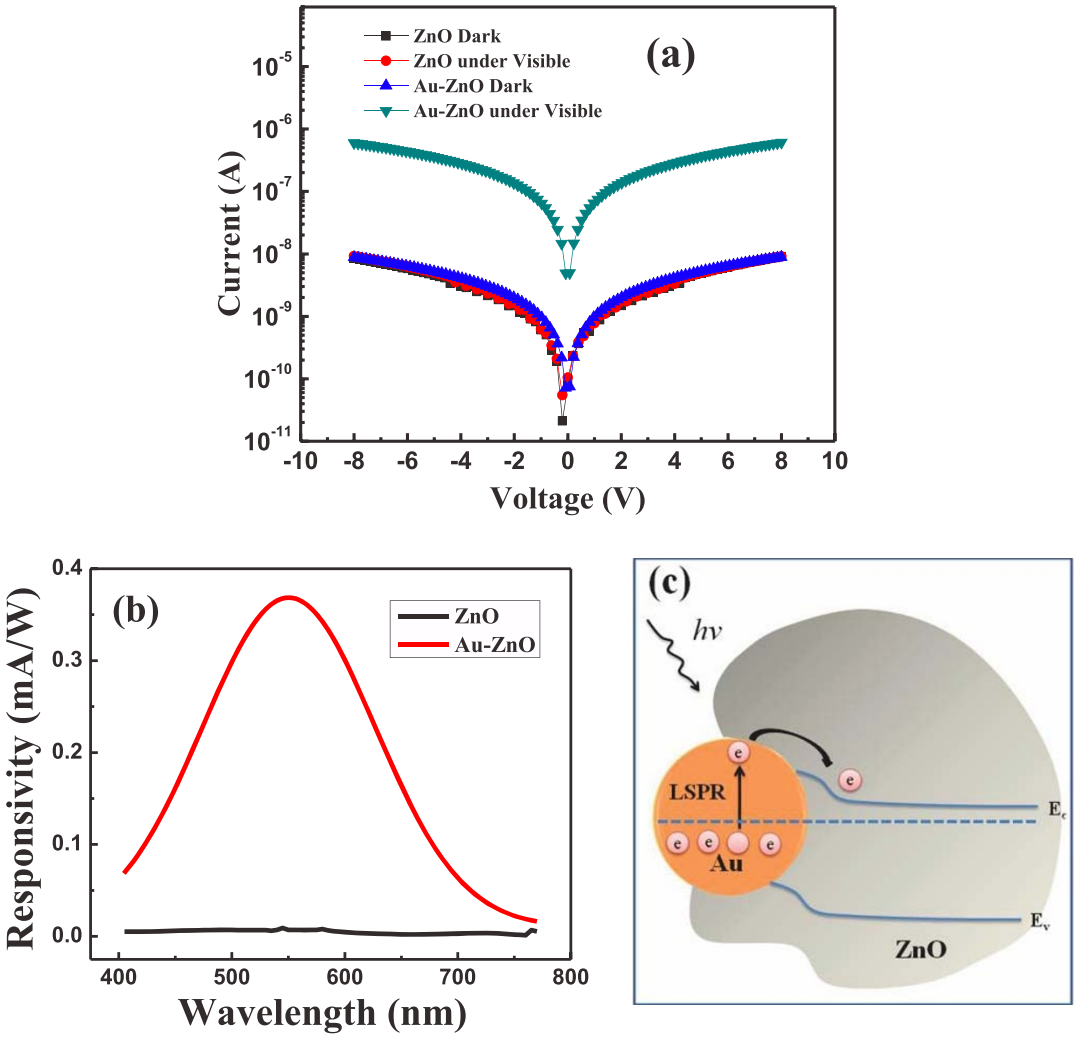


**Figure 7** | (a) I-V characteristics of ZnO and Au-ZnO devices under dark and visible light illumination. (b) Photoresponse of ZnO and Au-ZnO devices in the visible region at 5 V. (c) Schematic illustration of charge transfer process in Au-ZnO.

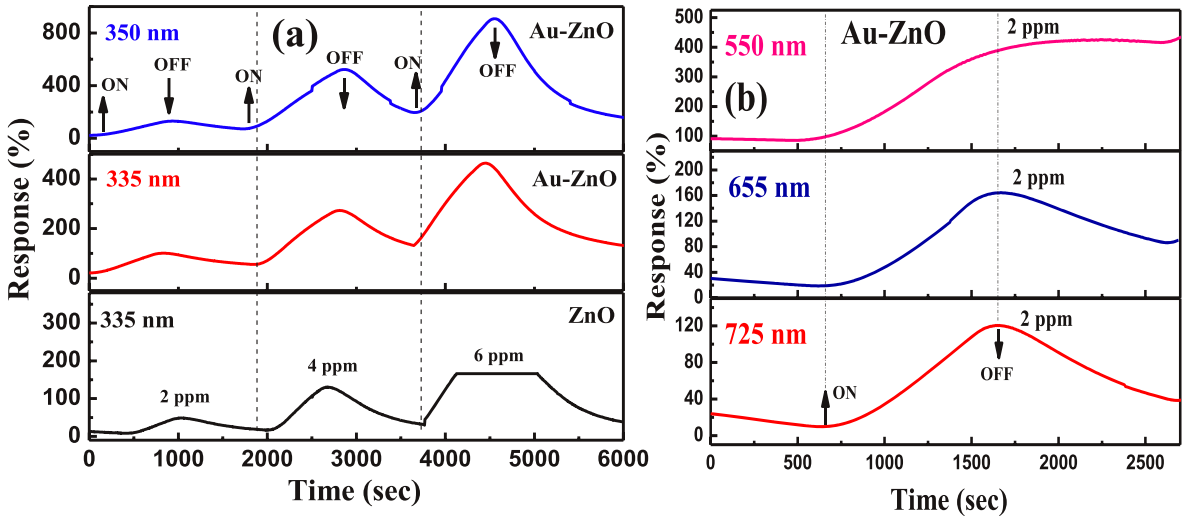


**Figure 8** | (a) Response of Au-ZnO and ZnO sensors to NO gas with various concentrations on illumination of UV wavelengths at room temperature. (b) Response of Au-ZnO sensor to NO gas on illumination of visible light at room temperature.

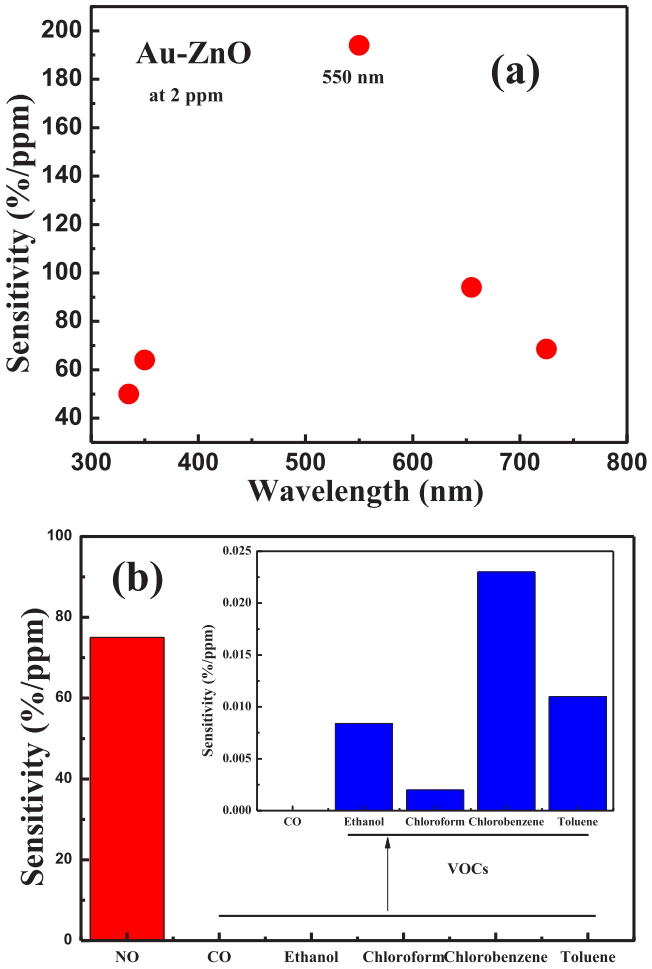


**Figure 9** | (a) Response of Au-ZnO sensor as a function of wavelength at 2 ppm NO concentration. (b) Histogram plot of Au-ZnO device sensitivity upon exposure to different gases. Inset shows the sensitivity to CO and other common VOCs.

a pronounced change in the response is observed even at very low part-per-million (ppm) concentration levels for both the devices. The sensing response of Au-ZnO device is significantly higher compared to ZnO device (enhanced by 3 times for 4 ppm NO) for 325 nm wavelength. The response of Au-ZnO device is also presented at different incident visible wavelengths upon exposure to NO gas at room temperature, as shown in Figure 8b. The response is found to be maximum for the device exposed to the wavelength of 550 nm. As observed from the Figure, the sensor response is restricted to lower ppm (2 ppm) levels because of the increased resistance at higher ppm levels at those wavelengths, which is higher than the instrumental detection limit (120 MΩ). On the other hand, the use of control ZnO device is also limited to UV illumination because of its negligible conductivity on exposure to visible wavelength, with energy below the band gap.

Figure 9a presents the sensitivity (defined as response per unit concentration of the gas or vapors) of Au-ZnO device as a function of wavelength at 2 ppm concentration of NO. The sensitivity is found to be maximum at 550 nm and decreases further at higher wavelength. The sensitivity at 2 ppm of NO gas is 194 and 50%/ppm for 550 nm and 335 nm wavelengths, respectively. To the best of authors' knowledge there is no data reported of NO gas sensing at room temperature on exposure to visible light using Au-ZnO nanocomposites. Most of the papers reported the sensing performance for $NO_2$ gas under UV irradiation at room temperature[24,26,27]. A histogram summarizing the selectivity of Au-ZnO sensor to NO gas

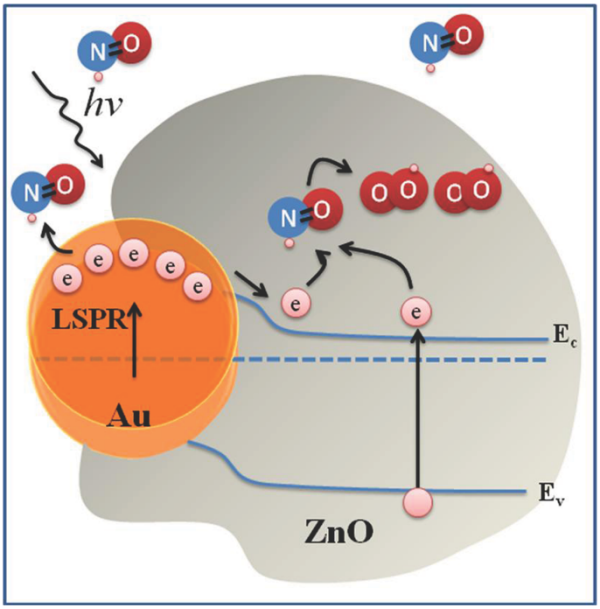


**Figure 10** | **Schematic illustration of NO gas sensing mechanism for Au-ZnO sensor in the presence of light.**

over CO and various volatile organic compounds is shown in Figure 9b. The Au-ZnO sensor displays much better sensing selectivity in presence of NO compared to other gases measured at 335 nm. The selectivity is found to be best at 335 nm compared to other wavelengths. This sensitivity is comparable in magnitude or even better than the conventional sensors reported using metal oxides operating at higher temperatures[19,42,43].

The lowest detection limit of NO using Au-ZnO sensors can be estimated in the following way[44].

$$rms_{noise} = \sqrt{\frac{V_x^2}{N}} \tag{3}$$

$$V_x^2 = \sum (y_i - y)^2 \tag{4}$$

where $rms_{noise}$ is the root mean square deviation of sensor noise in the relative conductance of the baseline, $y_i$ is the measured data points in the baseline (i.e. stable baseline before introducing the NO gas) and $N$ is the number of data points in the baseline. The measured data points ($y_i$) in the base line were plotted and a third order polynomial was fitted through these points. The values of $y$ were calculated using the fitting parameters. The detection limit (DL) has been calculated using the relation:

$$DL = 3 \times \frac{rms_{noise}}{slope} \tag{5}$$

Here, the slope has been obtained from the linear fit of the response versus concentration plot with a correlation coefficient of 0.99975 (Supplementary Figure S5). The detection limit of the NO gas sensing is found to be 0.1 ppb for Au-ZnO device using 335 nm. The capability of detection of very low concentration with high selectivity makes photoconductive Au-ZnO attractive for NO gas sensors.

**Mechanism of gas sensing.** Because of the large surface-to-volume ratio of ZnO nanostructures, oxygen molecules can be easily adsorbed on the surface, creating a depletion layer with lower conductivity ($O_2$(gas) + $e^-$ → $O_2^-$(adsorption)). Upon illumination, the electron-hole pairs are generated in the ZnO by absorbing the UV light and the photo-generated holes migrate to the surface along the potential gradient produced by band bending and oxygen is desorbed from the surface ($O_2^-$(adsorption) + $h^+$ →

$O_2$(gas)). This leads to an increase in the free carrier concentration and a decrease in the width of the depletion layer. When the gas flow is switched ON, NO molecules easily react with the photoelectrons generated in the ZnO because of its electron affinity. The reaction can be expressed by the following equation.

$$2NO + e^- = N_2(g) + O_2^- \quad (6)$$

Due to the interaction of NO molecules with electrons, the generated $O_2$ molecules are adsorbed on the surface of ZnO by capturing the photoelectrons, as shown in Figure 10. So the surface depletion layer in the ZnO nanosheet broadens again, which increase the resistance of the film. In case of Au-ZnO sample, additional interband electrons are provided by Au to interact with NO molecules, under the UV illumination. The excited interband electrons can flow to ZnO to increase the charge density or can directly interact with the NO molecules. The increased charge density of ZnO leads to the enhanced interaction with NO molecules, resulting in increased photo-resistance of Au-ZnO sensor NO, as shown in Figure 10.

On the other hand, the sensing mechanism in the visible region is primarily due to the localized surface plasmon response effect of Au. A large number of electrons oscillate on the surface of Au due to the resonance, when light interacts with it. This resonance is more sensitive to the charge density and dielectric environment of Au[45]. As already mentioned, NO molecule has strong electron affinity, which can easily adsorb on the surface of Au NPs to trap the electrons. As a result, the charge density of Au decreases, which eventually increases the resistance of the film. The NO gas molecules adsorbed on the surface of the Au-ZnO nanocomposite only contribute for sensing response. The sensing response in the UV region is enhanced mainly due to the photogenerated electrons in ZnO, with relatively less contribution from electrons of Au. Since the LSPR is predominantly a surface effect in the presence of visible light illumination, an enhanced interaction of the adsorbed NO gas molecules with electrons from Au are expected on the surface. The oscillating electrons of Au NPs due to LSPR have been reported to enhance the interaction with the adsorbed gas molecules[45]. Therefore, the sensing response is higher in the visible region compared to the UV one because of LSPR effect of Au NPs. These results suggest the potential of plasmonic Au-NP functionalized ZnO for light induced gas sensing applications at different wavelength (including the visible region) at room temperature.

## Conclusion

In conclusion, we demonstrated the operation of an efficient Au-ZnO UV photodetector and a plasmon enhanced NO gas sensor working at room temperature. The UV photoresponse of Au-ZnO nanocomposite is enhanced by 80 times over the control ZnO. This enhancement is attributed to the interband absorption or hole trapping ability of Au NPs within the nanocomposite, while the improved photoresponse in the visible region for Au-ZnO nanocomposite originates from the LSPR effect of Au NPs. The sensing response of Au-ZnO nanocomposite device is enhanced by three times at 4 ppm of NO gas under UV illumination over the control ZnO. The sensor response is found to be higher at visible wavelength region than the UV one, due to the plasmonic effect of Au NPs. The enhanced gas sensitivity of Au-ZnO nanocomposite both in UV and visible regions is due to the availability of copious electrons over the control ZnO. The sensitivity of Au-ZnO nanocomposite NO sensor is comparable or even better than the conventional ones based on metal oxides operated at higher temperatures reported in the literature. The sensor is found to be highly selective for NO over CO and other VOCs with a minimum detection limit of 0.1 ppb. The results suggest the potential use of Au-ZnO nanocomposite for gas sensors using plasmonic platform. The present study provides a novel platform for designing metal/wide band gap semiconductor nanocomposites for enhanced UV detection and wavelength tunable NO gas sensing operating at room tempearture by harvesting light in the visible region.

## Methods

**Preparation of ZnO nanostructures.** $Zn(NO_3)_2.6H_2O$ (6 g) was dissolved in 500 ml deionized (DI) water at room temperature in an ultrasonic bath. The NaOH solution (1.5 g in 10 ml DI water) was added drop wise to the $Zn(NO_3)_2.6H_2O$ solution under vigorous stirring at room temperature. The combined solution was heated at 200°C for 12 hrs. The extracted ZnO nanostructures from the solution were cleaned with DI water for 2 or 3 times and dried in air at 100°C.

**Preparation of Au-ZnO nanocomposites.** For preparation of Au-ZnO nanocomposites, 100 mg ZnO nanostructures were dispersed in DI water (100 mL) by strong sonication for 25 min and then 8 mL $HAuCl_4$ aqueous solution ($2.5 \times 10^{-3}$ M) was added to the above dispersion. The reaction mixture was kept under UV-light irradiation (365 nm) for 10 hrs. The prepared Au-ZnO material was centrifuged at 5000 rpm followed by washing it several times with DI water and drying at 100°C. Subsequently, the Au-ZnO material was annealed at 600°C for 1 hr in oxygen atmosphere, to obtain deep red color, indicating the formation of plasmonic Au-ZnO composite. A 1 μm thick Au-ZnO film was deposited on the interdigitated platinum electrodes ($0.64 \times 0.64$ cm$^2$) with inter-electrode separation 100 μm by spin coating for electrical measurements.

**Measurements.** The morphology of as-prepared nanocomposite was studied by transmission electron microscopy (TEM) (JEOL, JEM – 2100) with an incident energy 200 keV. The phase of Au-ZnO nanocomposite was analyzed by X-ray diffraction (XRD) (Philips, X-Pert MRD) at a grazing incident angle (~2.0°) using CuKα radiation. The chemical bonding of nanocomposite was studied using X-ray photoelectron spectroscopy (XPS) (ULVAC – PHI, INC, Japan) with a microfocused (100 μm, 25 W, 15 kV) monochromatic Al-Kα beam. The device was kept inside a sealed and transparent quartz window stainless steel chamber for gas sensing measurements. The electrical contacts to the sensor element were made using two probes connected with the chamber. The chamber had an inbuilt heater which was used to do the measurements at high temperature. The wavelength tunable sensing response was measured using a setup consisting of a broad band light source and a monochromator. Mass flow controllers (MFCs) were used to control the flow rates of carrier and test gases at appropriate proportion. These MFCs were controlled by a four channel power supply (MKS 247). The photo-resistance of gas sensors fabricated on interdigitated electrodes were measured using an Agilent 34972A LXI Data Acquisition (DAQ) unit fitted with 34901A 20 channel multiplexer switches and a digital ohm meter with a resolution of $0.1 \times 10^{-6}$ Ω. BenchLink Data Logger Pro software was used for data acquisition.


1. Mayer, K. M. & Hafner, J. H. Localized Surface Plasmon Resonance Sensors. *Chem. Rev.* **111**, 3828–3857 (2011).
2. Rodriguez-Lorenzo, L., de la Rica, R., Alvarez-Puebla, R. A., Liz-Marzan, L. M. & Stevens, M. M. Plasmonic Nanosensors with Inverse Sensitivity by Means of Enzyme-Guided Crystal Growth. *Nat. Mater.* **11**, 604–607 (2012).
3. Zheng, Y. B., Kiraly, B., Cheunkar, S., Huang, T. J. & Weiss, P. S. Incident-Angle-Modulated Molecular Plasmonic Switches: A Case of Weak Exciton-Plasmon Coupling. *Nano Lett.* **11**, 2061–2065 (2011).
4. Willets, K. A. & Duyne, R. P. V. Localized Surface Plasmon Resonance Spectroscopy and Sensing. *Annu. Rev. Phys. Chem.* **58**, 267–97 (2007).
5. Ozbay, E. Plasmonics: Merging Photonics and Electronics at Nanoscale Dimensions. *Science* **311**, 189–193 (2006).
6. Lu, L., Luo, Z., Xu, T. & Yu, L. Cooperative Plasmonic Effect of Ag and Au Nanoparticles on Enhancing Performance of Polymer Solar Cells. *Nano Lett.* **13**, 59–64 (2013).
7. Sobhani, A. *et al.* Narrow band Photodetection in the Near-Infrared with a Plasmon-Induced Hot Electron Device. *Nat. Commun.* **4**, 1643 (2013).
8. Li, D. *et al.* Realization of a High-Performance GaN UV Detector by Nanoplasmonic Enhancement. *Adv. Mater.* **24**, 845–849 (2012).
9. Choudhuri, B. *et al.* Enhanced photocurrent from generated photothermal heat in indium nanoparticles embedded $TiO_2$ film. *Appl. Phys. Lett.* **102**, 233108 (2013).
10. Liu, K., Sakurai, M., Liao, M. & Aono, M. Giant Improvement of the Performance of ZnO Nanowire Photodetectors by Au Nanoparticles. *J. Phys. Chem. C* **114**, 19835–19839 (2010).
11. Jean, J. *et al.* ZnO Nanowire Arrays for Enhanced Photocurrent in PbS Quantum Dot Solar Cells. *Adv. Mater.* **25**, 2790–2796 (2013).
12. Bai, S. *et al.* High-Performance Integrated ZnO Nanowire UV Sensors on Rigid and Flexible Substrates. *Adv. Funct. Mater.* **21**, 4464–4469 (2011).
13. Soci, C. *et al.* ZnO Nanowire UV Photodetectors with High Internal Gain. *Nano Lett.* **7**, 1003–1009 (2007).
14. Son, D. I. *et al.* Emissive ZnO–Graphene Quantum Dots for White-Light-Emitting Diodes. *Nat. Nanotech.* **7**, 465–471 (2012).
15. Jing, Z. & Zhan, J. Fabrication and Gas-Sensing Properties of Porous ZnO Nanoplates. *Adv. Mater.* **20**, 4547–4551 (2008).
16. Epifani, M. *et al.* Nanocrystalline Metal Oxides from the Injection of Metal Oxide Sols in Coordinating Solutions: Synthesis, Characterization, Thermal

Stabilization, Device Processing, and Gas-Sensing Properties. *Adv. Funct. Mater.* **16**, 1488–1498 (2006).
17. Rossinyol, E. *et al.* Synthesis and Characterization of Chromium-Doped Mesoporous Tungsten Oxide for Gas-Sensing Applications. *Adv. Funct. Mater.* **17**, 1801–1806 (2007).
18. Siemons, M., Leifert, A. & Simon, U. Preparation and Gas Sensing Characteristics of Nanoparticulate p-Type Semiconducting $LnFeO_3$ and $LnCrO_3$ Materials. *Adv. Funct. Mater.* **17**, 2189–2197 (2007).
19. Shishiyanu, S. T., Shishiyanu, T. S. & Lupan, O. I. Sensing characteristics of tin-doped ZnO thin films as $NO_2$ gas sensor. *Sensors and Actuators B* **107**, 379–386 (2005).
20. Bhattacharyya, P., Basu, P. K., Saha, H. & Basu, S. Fast response methane sensor using nanocrystalline zinc oxide thin films derived by sol–gel method. *Sensors and Actuators B* **124**, 62–67 (2007).
21. Pati, S., Maity, A., Banerji, P. & Majumder, S. B. Temperature dependent donor–acceptor transition of ZnO thin film gas sensor during butane detection. *Sensors and Actuators B* **183**, 172–178 (2013).
22. Huang, H. *et al.* Low-Temperature Growth of $SnO_2$ Nanorod Arrays and Tunable n–p–n Sensing Response of a ZnO/$SnO_2$ Heterojunction for Exclusive Hydrogen Sensors. *Adv. Funct. Mater.* **21**, 2680–2686 (2011).
23. Liu, X., Zhang, J., Guo, X., Wu, S. & Wang, S. Amino acid-assisted one-pot assembly of Au, Pt nanoparticles onto one-dimensional ZnO microrods. *Nanoscale* **2**, 1178–1184 (2010).
24. Lu, G. *et al.* UV-Enhanced Room Temperature $NO_2$ Sensor Using ZnO Nanorods Modified with $SnO_2$ Nanoparticles. *Sensors and Actuators B* **162**, 82–88 (2012).
25. Santra, S. *et al.* ZnO Nanowires Grown on SOI CMOS Substrate for Ethanol Sensing. *Sensors and Actuators B* **146**, 559–565 (2010).
26. Park, S., An, S., Mun, Y. & Lee, C. UV-Enhanced $NO_2$ Gas Sensing Properties of $SnO_2$-Core/ZnO-Shell Nanowires at Room Temperature. *ACS Appl. Mater. Interfaces* **5**, 4285–4292 (2013).
27. Mun, Y., Park, S., An, S., Lee, C. & Kim, H. W. $NO_2$ Gas Sensing Properties of Au-Functionalized Porous ZnO Nanosheets Enhanced by UV Irradiation. *Ceramics International* **39**, 8615–8622 (2013).
28. Zhai, J. *et al.* Enhancement of Gas Sensing Properties of CdS Nanowire/ZnO Nanosphere Composite Materials at Room Temperature by Visible-Light Activation. *ACS Appl. Mater. Interfaces* **3**, 2253–2258 (2011).
29. Rakshit, T., Mondal, S. P., Manna, I. & Ray, S. K. CdS-Decorated ZnO Nanorod Heterostructures for Improved Hybrid Photovoltaic Devices. *ACS Appl. Mater. Interfaces* **4**, 6085–6095 (2012).
30. Ono, L. K. & Cuenya, B. R. Formation and Thermal Stability of $Au_2O_3$ on Gold Nanoparticles: Size and Support Effects. *J. Phys. Chem. C* **112**, 4676–4686 (2008).
31. Dhara, S. & Giri, P. K. On the Origin of Enhanced Photoconduction and Photoluminescence from Au and Ti Nanoparticles Decorated Aligned ZnO Nanowire Heterostructures. *J. Appl. Phys.* **110**, 124317 (2011).
32. Gogurla, N., Mondal, S. P., Sinha, A. K., Katiyar, A. K., Banerjee, W., Kundu, S. C. & Ray, S. K. Transparent and flexible resistive switching memory devices with a very high ON/OFF ratio using gold nanoparticles embedded in a silk protein matrix. *Nanotechnology* **24**, 345202 (2013).
33. Li, L. *et al.* Single-Crystalline CdS Nanobelts for Excellent Field-Emitters and Ultrahigh Quantum-Efficiency Photodetectors. *Adv. Mater.* **22**, 3161 (2010).
34. Balamurugan, B. & Maruyama, T. Evidence of an Enhanced Interband Absorption in Au Nanoparticles: Size Dependent Electronic Structure and Optical Properties. *Appl. Phys. Lett.* **87**, 143105 (2005).
35. Xie, X. N. *et al.* UV-visible-near infrared photoabsorption and photodetection using close-packed metallic gold nanoparticle network. *J. Appl. Phys.* **107**, 053510 (2010).
36. Jin, Z., Gao, L., Zhou, Q. & Wang, J. High-performance flexible ultraviolet photoconductors based on solution-processed ultrathin ZnO/Au nanoparticle composite films. *Sci. Rep.* **4**, 4268 (2014).
37. Zhang, Z., Zhang, L., Hedhili, M. N., Zhang, H. & Wang, P. Plasmonic Gold Nanocrystals Coupled with Photonic Crystal Seamlessly on $TiO_2$ Nanotube Photoelectrodes for Efficient Visible Light Photoelectrochemical Water Splitting. *Nano Lett.* **13**, 14–20 (2013).
38. Pu, Y.-C. *et al.* Au Nanostructure-Decorated $TiO_2$ Nanowires Exhibiting Photoactivity Across Entire UV-visible Region for Photoelectrochemical Water Splitting. *Nano Lett.* **13**, 3817–3823 (2013).
39. Yun, H. J. *et al.* A Combination of Two Visible-Light Responsive Photocatalysts for Achieving the Z-Scheme in the Solid State. *ACS Nano* **5**, 4084–4090 (2011).
40. de Arquer, F. P. G., Mihi, A., Kufer, D. & Konstantatos, G. Photoelectric Energy Conversion of Plasmon-Generated Hot Carriers in Metal-Insulator-Semiconductor Structures. *ACS Nano* **7**, 3581–3588 (2013).
41. Mubeen, S., Hernandez-Sosa, G., Moses, D., Lee, J. & Moskovits, M. Plasmonic Photosensitization of a Wide Band Gap Semiconductor: Converting Plasmons to Charge Carriers. *Nano Lett.* **11**, 5548–5552 (2011).
42. Koshizaki, N. & Oyama, T. Sensing characteristics of ZnO-based NO sensor. *Sensors and Actuators B* **66**, 119–122 (2000).
43. Navale, S. C., Ravi, V., Mulla, I. S., Gosavi, S. W. & Kulkarni, S. K. Low temperature synthesis and NO sensing properties of nanostructured Al-doped ZnO. *Sensors and Actuators B* **107**, 379–386 (2005).
44. Ammu, S. *et al.* Flexible, All-Organic Chemiresistor for Detecting Chemically Aggressive Vapors. *J. Am. Chem. Soc.* **134**, 4553–4556 (2012).
45. Joy, N. A., Rogers, P. H., Nandasiri, M. I., Thevuthasan, S. & Carpenter, M. A. Plasmonic-Based Sensing Using an Array of Au−Metal Oxide Thin Films. *Anal. Chem.* **84**, 10437–10444 (2012).

## Acknowledgments

The experimental facilities of the DST 'FIST' and 'GPU' projects are gratefully acknowledged. One of the authors (S. Santra) acknowledges the Department of Science and Technology (DST), India for the support of the work (project no SR/S2/RJN-104/2011).

## Author contributions

N.G. and A.K.S. performed synthesis of Au-ZnO nanocomposites and characterizations. N.G. and S.S. carried out sensor measurements. N.G., S.S., S.M. and S.K.R. analyzed and interpreted the data. N.G. and S.S. wrote the manuscript. S.K.R. supervised the entire manuscript preparation. All the authors participated in discussion of the research.

## Additional information

**Supplementary information** accompanies this paper at http://www.nature.com/scientificreports

**Competing financial interests:** The authors declare no competing financial interests.

**How to cite this article:** Gogurla, N., Sinha, A.K., Santra, S., Manna, S. & Ray, S.K. Multifunctional Au-ZnO Plasmonic Nanostructures for Enhanced UV Photodetector and Room Temperature NO Sensing Devices. *Sci. Rep.* **4**, 6483; DOI:10.1038/srep06483 (2014).